Research Article

Essam B. Moustafa, A. Melaibari, Ghazi Alsoruji, Asmaa M. Khalil, and Ahmed O. Mosleh*

# Al 5251-based hybrid nanocomposite by FSP reinforced with graphene nanoplates and boron nitride nanoparticles: Microstructure, wear, and mechanical characterization

https://doi.org/10.1515/ntrev-2021-0108
received August 27, 2021; accepted October 8, 2021

**Abstract:** The strength and wear resistance of aluminium alloys must be improved to enhance their usage in lightweight constructions. Thus, in this study, graphene nanoplates (GNPs) and boron nitride (BN) nanoparticles were reinforced into the Al 5251 aluminium alloy by friction stir processing (FSP). The Al 5251 aluminum alloy sheets were patterned with holes and filled by mono GNPs, mono BN nanoparticles and a hybrid of BN nanoparticles and GNPs. The microstructure, wear, and mechanical properties of the as-received, after FSP, and the manufactured surface nanocomposites were analysed. Wear tests were performed using two methods: weight loss and volume loss methods. FSP led to four times grain refinement. Due to the Zener pinning effect, the reinforcement nanoparticles improved the grain refinement effect by seven times decrease in the mean grain size. The wear rate by volume and weight loss with reinforcing BN nanoparticles decreased by 160 and 1,340%, respectively. Note that the GNP reinforcement insignificantly improved the wear resistance and hardness compared with the BN nanoparticles. The hardness was increased by 50, 120, and 80% by reinforcing the Al 5251 alloy with GNPs, BN, and a hybrid of BN nanoparticles and GNPs, respectively. The nanocomposite reinforced with GNPs exhibited superior mechanical properties compared to the other nanocomposites.

**Keywords:** nanocomposites, friction stir processing, hybrid nanocomposite, Al 5251, graphene nanoplates, boron nitride, wear

*** Corresponding author: Ahmed O. Mosleh,** Mechanical Engineering Department, Shoubra Faculty of Engineering, Benha University, Cairo, 11629, Egypt, e-mail: ahmed.omar@feng.bu.edu.eg, mosleh@misis.ru
**Essam B. Moustafa, Ghazi Alsoruji:** Mechanical Engineering Department, Faculty of Engineering, King Abdulaziz University, P.O. Box 80204, Jeddah, Saudi Arabia
**A. Melaibari:** Mechanical Engineering Department, Faculty of Engineering, King Abdulaziz University, P.O. Box 80204, Jeddah, Saudi Arabia; Center of Nanotechnology, King Abdulaziz University, Jeddah, 21589, Saudi Arabia
**Asmaa M. Khalil:** Mechanical Engineering Department, Shoubra Faculty of Engineering, Benha University, Cairo, 11629, Egypt

## Nomenclature

| | |
|---|---|
| $Al_2O_3$ | aluminum oxide |
| AMMCs | metal matrix composite |
| AS | advancing side |
| BM | base metal |
| BN | boron nitride |
| CNT | carbon nanotube |
| DRX | dynamic recrystallization |
| FSP | friction stir processing |
| GNPs | graphene nanoplates |
| HAZ | heat-affected zone |
| MWCNT | multiwall carbon nanotube |
| NG | nugget zone |
| OM | optical microscopy |
| RS | retreating side |
| SD | standard deviation |
| SEM | scanning electron microscopy |
| SiC | silicon carbide |
| SZ | nugget or stirred zone |
| TEM | transmission electron microscopy |
| TMAZ | thermomechanical affected zone |
| UTS | ultimate tensile strength |
| WC | tungsten carbide |

## 1 Introduction

Graphene is a two-dimensional single-layer crystalline material composed of carbon atoms. Its unique mechanical,

electrical, and thermal properties have recently attracted considerable research attention [1–4]. Because of its large aspect area ratio, superior thermal and mechanical properties, and lightweight, graphene is incorporated as a practicable reinforcement material for aluminium metal–matrix composites (AMMCs) [5–7]. However, the dispersion of graphene in an AMMC is a major challenge in the fabrication of the nanocomposite matrix. Owing to its elastic incompatibility, the loss of interface bonding at the graphene/aluminium matrix creates a weak interfacial adhesion and degrades the AMMC's mechanical performance. Graphene is exceptionally hard compared with other reinforcements due to its high interfacial surface [4,8–10]. In contrast, due to its good thermal, mechanical, and physical properties, in addition to its excellent lubricating property, boron nitride (BN) nanoparticles are most commonly used for strengthening AMMCs [11,12].

Despite their high specific strength and superior thermal and electrical conductivities, aluminium-based alloys have limited application due to their low hardness and poor wear resistance. Their tribological properties can be significantly enhanced by reinforcing them with ceramic nano/microparticles. These reinforcements exhibit high wear and hardness characteristics and significantly improve the base aluminium alloys' mechanical performance [13]. For example, tungsten nanoparticles were used to reinforce Al 5182 alloy using friction stir welding; the fabrication processes, which were carried out at different traverse speeds, revealed an indirect relation between the reverse tool speed and ultimate tensile strength. In contrast, the nugget zone's hardness is directly proportional to the tool traverse speed [14].

Graphene is one of the most common reinforcing nanoparticles used to fabricate metal–matrix nanocomposites. The friction and wear resistance properties of the Al 5000 series are enhanced by impeding graphene nanoplates (GNPs) into the base alloy through friction stir processing (FSP). In addition, GNPs are incorporated into the Al–Mg alloy to improve its tensile strength and obtain microstructure grain refinement. Due to the generation of a lubricant layer during the sliding surfaces' FSP, the addition of GNPs reduces the friction coefficient by up to 60% compared to that of the base alloy [15,16].

The hybrid composite matrix of Al 5056_SiC_bagasse ash was fabricated using the stir cast method. The addition of 3% silicon additives did not significantly affect the composite matrix; hence, it did not increase the hybrid composite's hardness; even the addition of 10% additive did not have any significant effect. In contrast, the wear resistance was increased by the addition of a low percentage of bagasse ash [17]. Fabricating an AMMC with uniformly distributed reinforcing particles has a been major challenge recently. FSP is an efficient technique for producing fully homogenized stirred nanocomposite materials [18–22].

The processing parameters of FSP have a significant impact on the mechanical properties and microstructural behaviour of AMMCs; thus, significant efforts have been made to establish a relation between the FSP parameters and the structure and properties of fabricated AMMCs [23–25]. The wear and hardness properties of the hybrid composite materials were significantly improved owing to the superior properties of the reinforcement components. However, these particles also produced some undesirable effects, such as decreased strain, ductility, and deformability [26–28]. In the case of composites fabricated by FSP, hybrid reinforcements were employed to improve the surface characteristics of the Al matrix by impeding different types of reinforcement particles into the base matrix [29–31]. The combination of two different types of reinforced particles improved the microhardness, strength, and wear resistance of the manufactured composite [32,33]. Therefore, in the current study, two distinct reinforced nanoparticles, GNPs and BN nanoparticles were used to create hybrid metal–matrix nanocomposites. The literature has focused on the microstructure and mechanical characteristics of nanocomposites. However, the effects of hybrid nanoparticles on the tribological and mechanical characteristics of the hybridization matrices subjected to FSP have not been studied.

We studied the Al 5251 AMMCs reinforced with mono BN nanoparticles, mono GNPs, and hybrid GNPs and BN nanoparticles and fabricated them using the FSP technique. In addition, we compared the fabricated composites and as-received samples subjected to FSP based on microstructural analysis, tribological behaviour, and mechanical properties to identify the most influential reinforcement that significantly impacts the wear behaviour besides the refinement and mechanical properties. This research aims to study how incorporating two different reinforcement nanoparticles belonging to the same family impacts the fabricated metal–matrix nanocomposite.

## 2 Experimental work

Al 5251 alloy was used as the matrix for the fabricated nanocomposites. The chemical composition of this alloy is shown in Table 1.

FSP was used to manufacture the surface nanocomposite on the Al 5251 aluminium alloy plates prepared

**Table 1:** Chemical composition of Al 5251 aluminium alloy (wt%)

| Mg | Fe | Cr | Mn | Ti | Si | Cu | Al |
|---|---|---|---|---|---|---|---|
| 1.83 | 0.55 | 0.21 | 0.058 | 0.03 | 0.2 | 0.1 | Remain |

and machined using a milling machine (Bridgeport, Elmira, NY, USA) to create a set of holes in a linear pattern, as shown in Figure 1(a).

Two scenarios were used to insert GNPs and BN nanoparticles into the grooved holes: the first scenario used a single additive (mono nanocomposites) and the second scenario used a mixture of GNPs and BN nanoparticles (hybrid nanocomposite). The hybrids were equally divided and well-stirred into the mixture before being inserted into the base matrix holes. FSP was conducted on an automated milling machine under the following conditions: the tilt angle was set to 1°, the linear travelling speed was 30 mm/min, and the tool rotation speed was 1,125 rpm. The stirring action was performed with a triangular pin tool. The design and dimensions of the tool are illustrated in Figure 1(b).

Transmission electron microscopy (TEM; JEOL, Tokyo, Japan) was used to examine the parameters of GNPs and BN nanoparticles (Figure 2). The average particle size of the BN nanoparticles was 100 ± 5 nm, and the GNPs were 7 ± 0.6 nm thick and 5 ± 0.5 µm wide. The BN nanoparticles and GNPs used in this study were purchased from Nanoshel-UK-Ltd. Company (Congleton, UK) with a purity of >99%. The total volume of the manufactured surface nanocomposite can be computed using equations (1) and (2):

$$V_C = V_p + V_m, \tag{1}$$

$$V_C = \text{Projected area of tool} \times \text{Length of the manufactured composite}. \tag{2}$$

The volume of the used nanoceramics and the matrix can be calculated using equations (3) and (4):

$$V_p = \text{No of holes} \times \text{Volume of each hole}, \tag{3}$$

$$V_m = V_c - V_p. \tag{4}$$

The volume fraction of the used nanoceramics and the matrix can be calculated using equations (5) and (6):

$$VF_p = \frac{V_p}{V_C}, \tag{5}$$

$$VF_m = \frac{V_m}{V_C}. \tag{6}$$

The volume $V_p = 0.42\,cm^3$ of the nanoceramic particles and that of the manufactured composite was $V_C = 3.75\,cm^3$; thus, the volume of the matrix was calculated as $V_m = 3.33\,cm^3$. Therefore, the volume fraction of the reinforced nanoceramics within the matrix was 11.6%.

The microstructures of the as-received and processed samples were analysed. The samples were partitioned perpendicular to the processing direction, mechanically ground, polished, and etched using metallurgical standard agents. The prepared samples were analysed using an optical microscope Olympus (Olympus BX51, Miami, FL, USA) and a scanning electron microscope (Tescan Brno s.r.o., Kohoutovice, Czech Republic) coupled with an energy dispersive spectrometer (EDS, X-MAX80) system. Vickers micro-hardness tests were conducted using a ZwickRoell

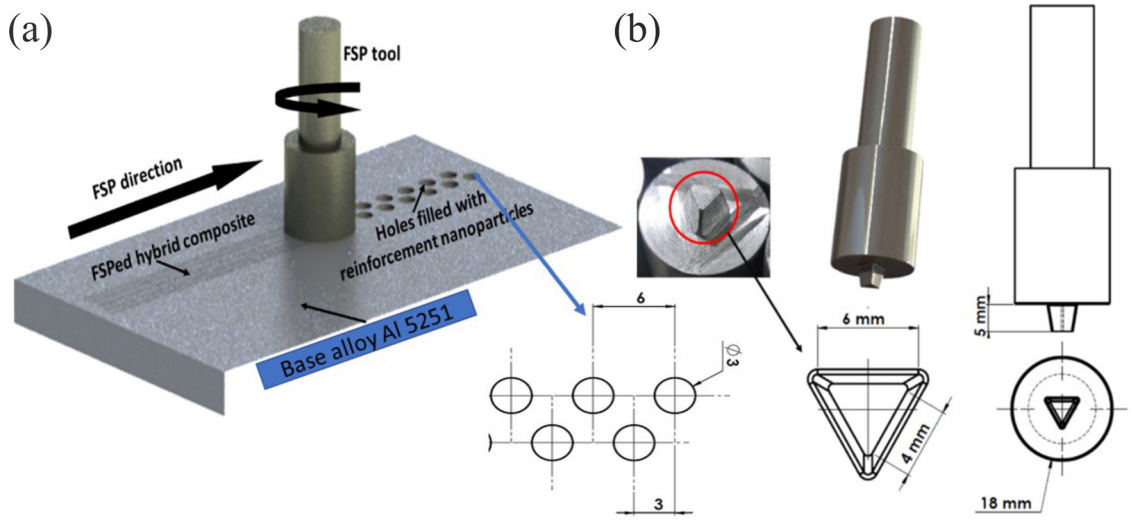


**Figure 1:** (a) Schematic of the fabrication process of the nanocomposite and (b) tool design used for FSP. All dimensions are in mm.

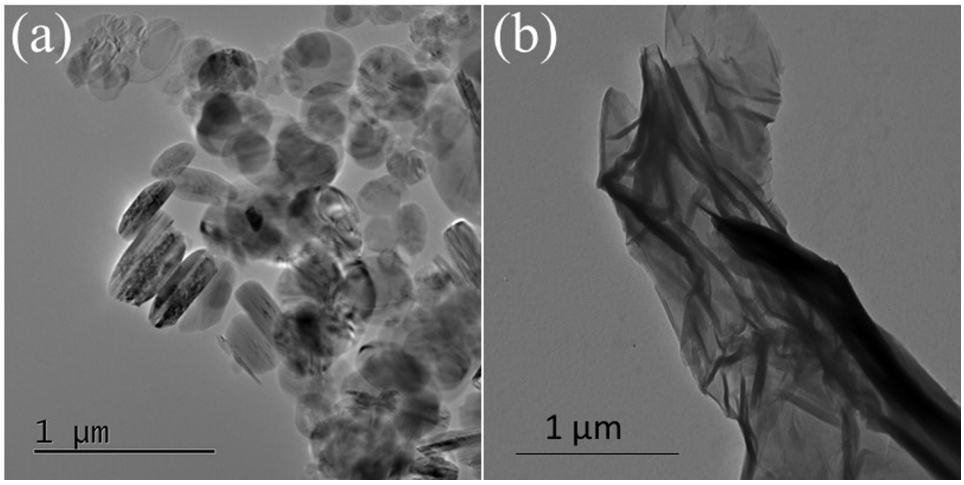


**Figure 2:** TEM images of (a) BN nanoparticles and (b) GNPs.

(Zwick/Roell, Kennesaw, GA, USA) testing mashing, as per the ASTM E-384-17 standard. Before the hardness test, the samples were ground and polished. Vickers micro-hardness measurements were taken throughout the sample surface in all processing regions to create the hardness profile.

The wear tests were performed using two different methods to ensure the wear behaviour of the hybrid composite metal matrix. The first technique was based on the wear volume loss rate, and the second method used the weight loss technique. The wear behaviour of the base sample fabricated by FSP was evaluated using a pin-on-disk tribometer (CSM Instruments SA Rue de la Gare 42034 Peseux - Switzerland) tester with the volume loss technique at room temperature. The weight loss rate of wear was determined using the TNO equipment (Delft, The Netherlands). The specimens were weighed and measured using a digital scale with a 0.0001 g precision. All samples were polished with various grades of SiC grinding papers ranging from 600 to 4,000. The test was carried out at a constant load of 10 N. The radius of the travelling pin was 2 mm, and the linear speed was 0.1 cm/s. The friction coefficient was calculated from the normal load ratio and the friction force between the steel pin and sample. In contrast, the worn track was measured by a Stylus Profiler System (Dektak XTL Stylus Profiler System, Bruker, Bremen, Germany) at different locations through the wear track. An optical microscope was used to examine the worn track at high magnifications to determine the wear behaviour of different fabricated samples.

The tensile tests were performed using a Zwick/Roell Z250 all-round series testing machine (Zwick/Roell, Kennesaw, GA, USA) according to ASTM B557M-15 [34]. Three tensile samples of each composite were tested (Figure 2d), and the average of these three data points was used to obtain the reported value.

# 3 Results and discussion

## 3.1 Microstructural analysis

Figure 3 illustrates the micrographs of the as-received Al 5251 alloy, the cross-sections of the samples subjected to FSP, and the statistical quantity analysis of the grains.

The as-received Al 5251 alloy exhibited elongated grains with an average grain size of 60 µm and a standard deviation (SD) of 25 µm. The aspect ratio of the grains in the as-received state was 1.8. The high SD value suggested nonuniform grain size distribution (Figure 3e). The FSP zone structure was composed of (1) nugget or a stirred zone (SZ), (2) thermomechanical-affected zone, and (3) thermal-affected zone (Figure 4a). During FSP, owing to friction and severe plastic deformation, the SZ was heated intensely, resulting in a dynamically recrystallized (DRX) microstructure with a mean grain size of 15 µm and an SD of 4 µm. Therefore, the SZ exhibited a more uniform, equiaxed (aspect ratio = 1.03), and fine-grained structure than the as-rolled sheet (Figure 3b and c). The SZ grains were typically distributed in size, reflecting the structure's homogenization during FSP (Figure 3f).

Figure 4 shows the SZ's microstructure, reinforced with GNPs, BN nanoparticles, and hybrid BN nanoparticles + GNPs, and the grains' statistical quantity analysis.

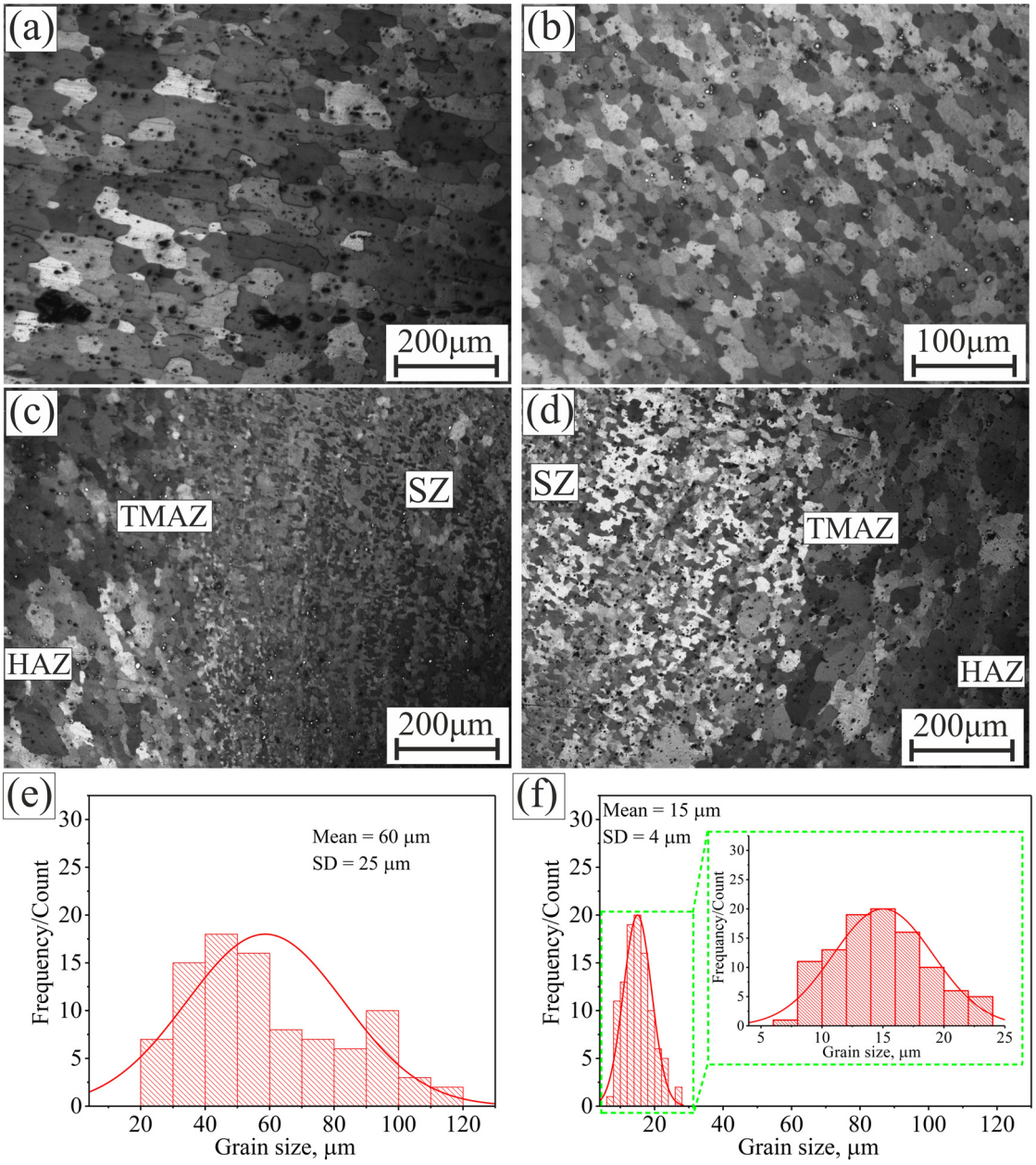


**Figure 3:** Microstructure of (a) as-received Al 5251 alloy, (b) after FSP, (c) advancing side, and (d) retreating side; (e) grain size distribution of the as-received alloy and (f) grain size distribution of SZ after FSP.

Reinforcing the base metal with different nanoparticles changed the grain morphology and size. Generally, AMMCs demonstrate a finer and more equiaxed grain structure (Figure 4a, c and, e). The SDs of the grain size of the AMMCs were 3.5, 3.7, and 3.7 μm for mono GPNs (Figure 4b), mono BN nanoparticles (Figure 4d), and the hybrid of BN nanoparticles + GNPs (Figure 4f), respectively. The grains were normally distributed about the mean value, which suggested the homogenous distribution of the equiaxed grains. The aspect ratio of the grains in all manufactured composites was the same (*i.e.* 1.02).

Figure 5 illustrates the mean grain sizes for the as-rolled alloy and friction SZ of the primary material and the studied AMMCs. Reinforcing particles improved the grain refining effect in the SZ. The mean grain sizes of the mono GPNs, mono BN nanoparticles, and hybrid of BN nanoparticle + GNPs were 11.2 ± 3.5, 12.3 ± 3.7, and 13.0 ± 3.7 μm, respectively. Under the Zener pinning effect, the nanoparticles inhibited grain growth during DRX, resulting in a more refined grain structure formation.

Figure 6 shows the SEM micrographs of the studied nanocomposites in the friction SZ. The bonding among

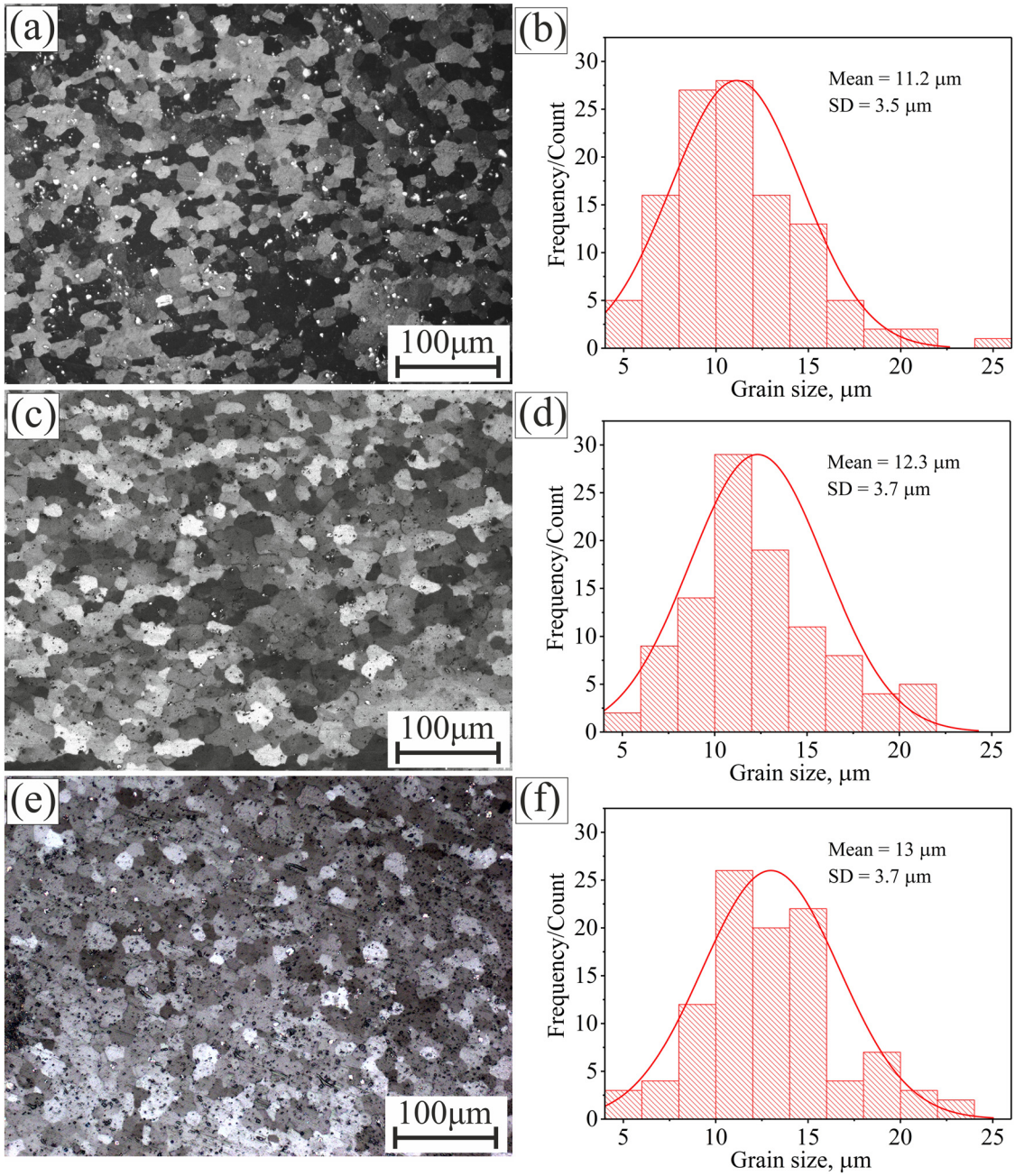


**Figure 4:** Microstructure and frequency distribution of the grain size of the matrix alloy reinforced with (a and b) mono GNPs, (c and d) mono BN nanoparticles, and (e and f) hybrid of BN nanoparticles and GNPs.

AMMCs, BN nanoparticles, and GNPs was observed. The EDS spectra analysis was performed on all SEM images of the manufactured surface nanocomposites (Figure 6). The EDS results confirmed the presence of both reinforcements in the hybrid composite. The BN distribution in the Al 5251_BN composite was uniform after FSP, whereas GNPs were not uniformly distributed in the manufactured composite due to their lubricating nature during FSP (Figure 6a and b). This causes a lack of dispersion for GNPs; hence, it is expected to influence the hardness and mechanical properties of the manufactured AMMCs. The nanocomposite matrix of hybrid Al 5251_BN + GNPs was affected by GNP distribution; however, the BN nanoparticles were dispersed well in the matrix (Figure 6c). The SEM images were scanned at two different magnifications: the main image was captured at low magnification of 7,500×, and the subset figures were scanned at a high magnification of 15,000×.

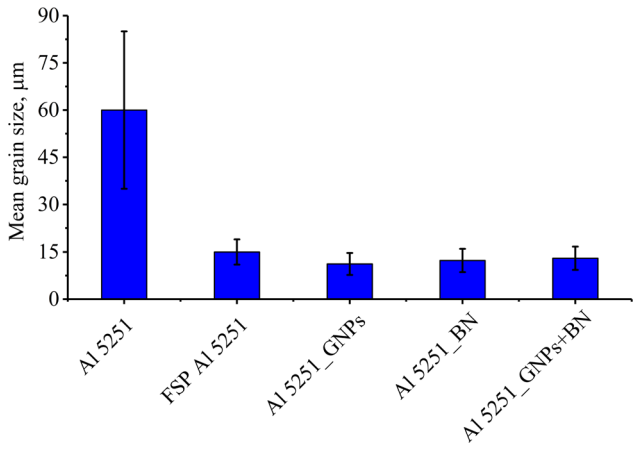


**Figure 5:** Average grain size of the as-received BM and friction SZ without and with different reinforcements nanoparticles.

The EDS mapping analysis was conducted to examine the distribution of reinforcements, as well as the undesired nanoclusters, and the agglomeration of the reinforced nanoparticles. Figure 7 shows the EDS mapping after FSP in the SZ without reinforcements (Figure 7a) and with reinforcement with GNPs (Figure 7b), BN nanoparticles (Figure 7c), and a hybrid of GNPs and BN nanoparticles (Figure 7d). The EDS maps reveal the existence of reinforced particles in the SZ in addition to the alloy's major alloying components and phases. All samples showed a uniform distribution of reinforcement nanoparticles inside the SZ, with no evidence of significant clustering.

## 3.2 Microhardness

Figure 8 shows the Vickers microhardness profiles and a mean value for the as-processed Al 5251 alloy and the SZ of the basic alloy and the studied AMMCs. The as-processed BN nanoparticles exhibited an average Vickers microhardness of 52 ± 2 HV. The hardness of the samples subjected to FSP was increased (63 ± 3 HV) due to good dispersion and distribution of $Mg_2Al_3$ intermetallic precipitates [35] (Figure 8b). The hardness in the composite area increased significantly. The average values of the measured microhardness in the SZ of the composite layer reinforced by mono GNPs, mono BN nanoparticles, and a hybrid of BN nanoparticles + GNPs were 75 ± 3, 112 ± 4, and 93 ± 4 HV, respectively. The enhancement in hardness was attributed to the grain structure refining and the presence of hard particles. The nanocomposite reinforced with BN nanoparticles exhibited the highest hardness values, followed by that reinforced with a hybrid of BN nanoparticles and GNPs, and then GNP nanocomposite. The mean grain size significantly impacts the enhancement of hardness based on the Hall–Petch relation. The homogeneity of AMMC grains after FSP also improved the hardness in the SZ.

## 3.3 Mechanical properties

Figure 9 illustrates the stress–strain curves and mechanical properties of AMMCs before and after FSP and those of the manufactured nanocomposites. Each set of data is the average of three specimens. The Al 5251 aluminium alloy sheets exhibited yield strength, tensile strength, Young's modulus, and elongation to failure of 66 MPa, 171 MPa, 64 GPa, and 15.3%, respectively (Figure 9a and b). After FSP, the microstructure of the processed zone was enhanced, resulting in improvement in the mechanical properties and plasticity; the elongation to failure was increased to 18%. Moreover, finer grains and increased grain boundaries resulted in stronger resistance to dislocation motion. The Hall–Petch equation describes the strengthening mechanism by the grain boundary; this was achieved after FSP. The reinforcing of the nanoparticles within the matrix significantly enhanced the mechanical properties of the manufactured composites, indicating a significant impact of the nanoparticles on the manufactured nanocomposites. However, this reinforcement decreased the plasticity. The yield strength and modulus of elasticity were enhanced for all manufactured nanocomposites. The nanoparticles present in the SZ acted as obstacles for dislocation motions, increasing the mechanical properties of the manufactured composites. The large specific surface area of GNPs led to good interfacial adhesion between them and the matrix, which improved the mechanical properties of Al 5251_GNPs and the Al 5251_BN + GNP nanocomposite. The maximum ultimate tensile strength was obtained for the nanocomposite reinforced with GNPs.

## 3.4 Wear behaviour

The wear test was carried out using a tribometer tester to calculate the wear rate and coefficient of friction (COF). At the beginning of the test, the wear rate results recorded a short transient response and then reached steady-state wear rate behaviour, as shown in Figure 10. As shown in the COF profile of the worn track section, the base Al 5251 alloy and the manufactured composite reinforced with mono GNPs showed a maximum COF value (0.48)

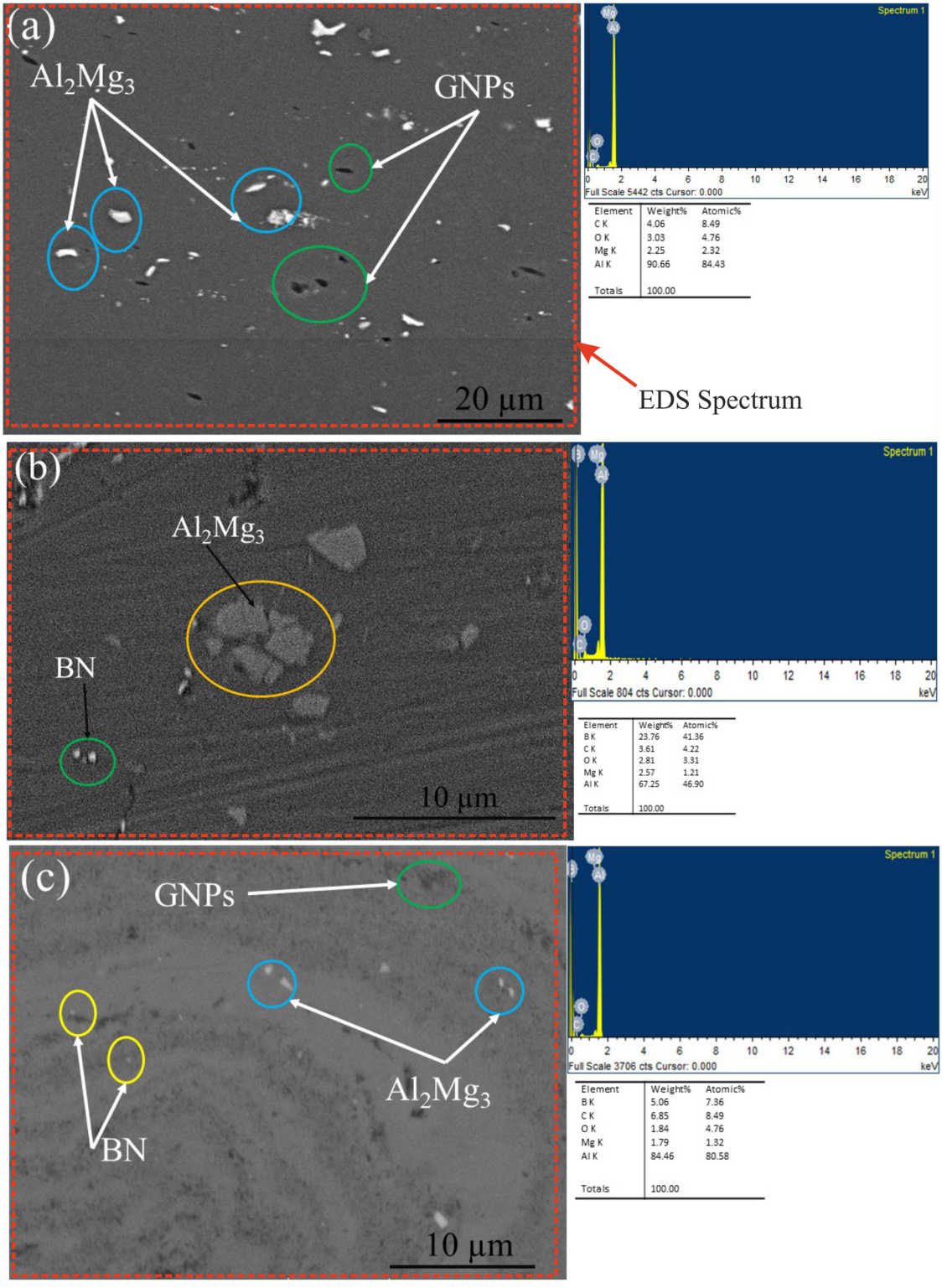


**Figure 6:** SEM image of the fabricated nanocomposites: (a) Al 5251_GNPs, (b) Al 5251_BN, and (c) Al 5251_BN + GNPs.

(Figure 10a and b). In contrast, the composite reinforced with mono BN nanoparticles demonstrated a minimum COF value (0.32). This effect can be attributed to the nature of the BN particles as a self-lubricant during sliding wear action [36]. The adhesion behaviour between the Al 5251_BN surface nanocomposite and the sliding wear tool is

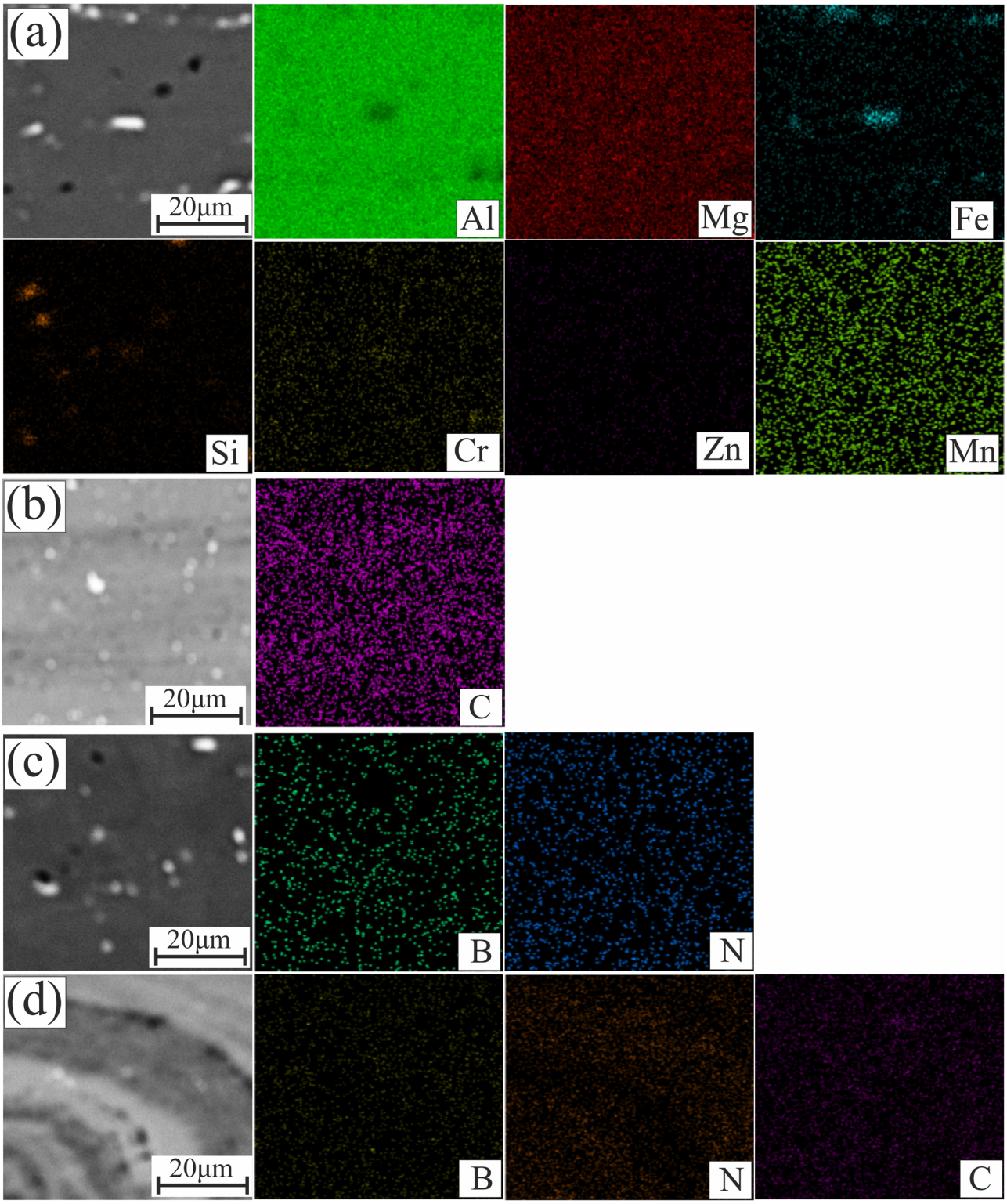


**Figure 7:** EDS mapping analysis in SZ (a) after FSP without reinforcements and reinforced with (b) GNPs, (c) BN nanoparticles, and (d) hybrid of GNPs and BN nanoparticles.

minimized due to BN's lubrication effect. This explanation of abrasive wear type is illustrated in refs [37,38]. The COF value for the Al 5251_GNP surface nanocomposite was very close to that for the base alloy. Therefore, despite GNPs being considered a lubricant [39], they insignificantly influence the wear behaviour. The reinforcement dispersion and its

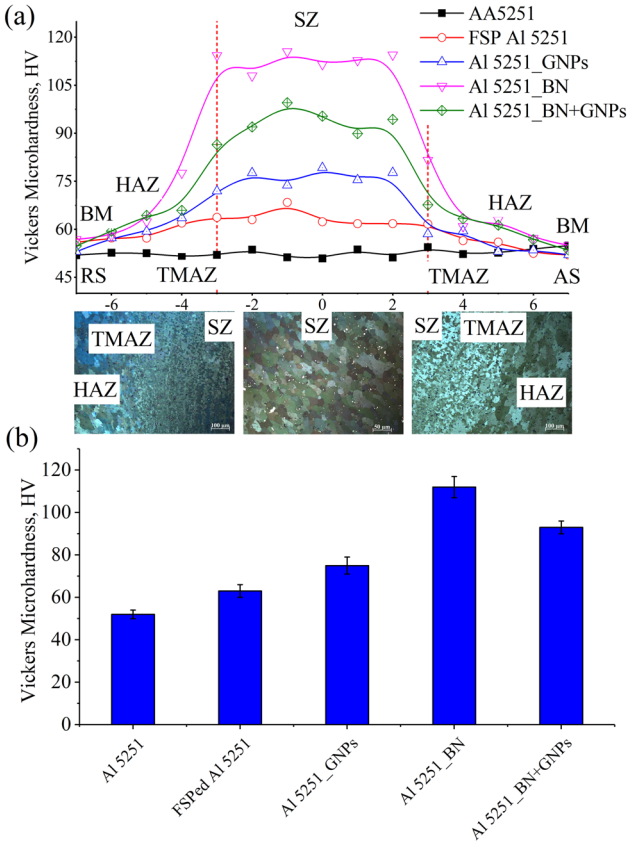


**Figure 8:** (a) Vickers microhardness profile and (b) the average Vickers microhardness in the BM and the SZ.

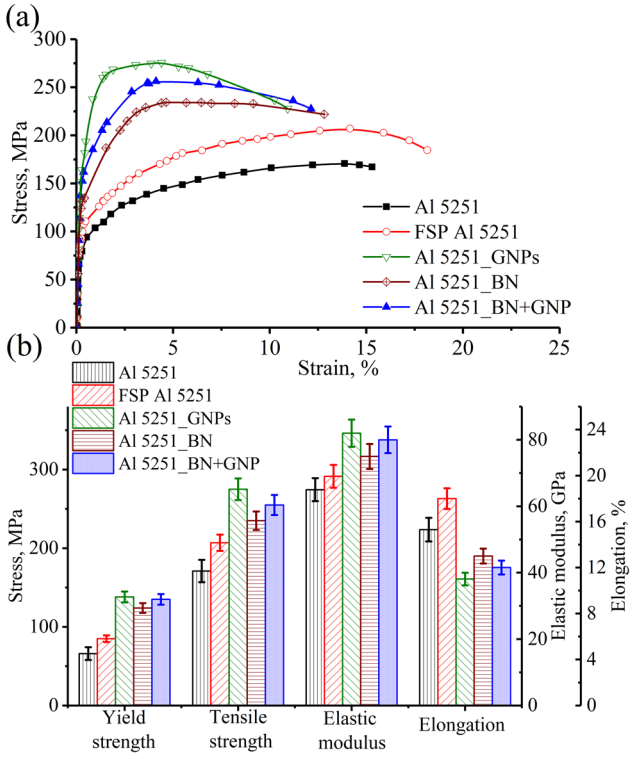


**Figure 9:** (a) True stress-strain curves; (b) tensile properties of the investigated hybrid composites.

distribution after FSP have a major effect on the microstructure and mechanical, wear, and hardness properties of the fabricated composites. The COF value of the Al 5251_BN + GNP nanocomposite lies in the middle of the COF values of mono GNPs and the mono BN surface nanocomposite.

The wear rates for the investigated Al 5251 alloy decreased with the addition of reinforcement particles. There is a direct relationship between the wear rate and hardness behaviour of composite materials; hard

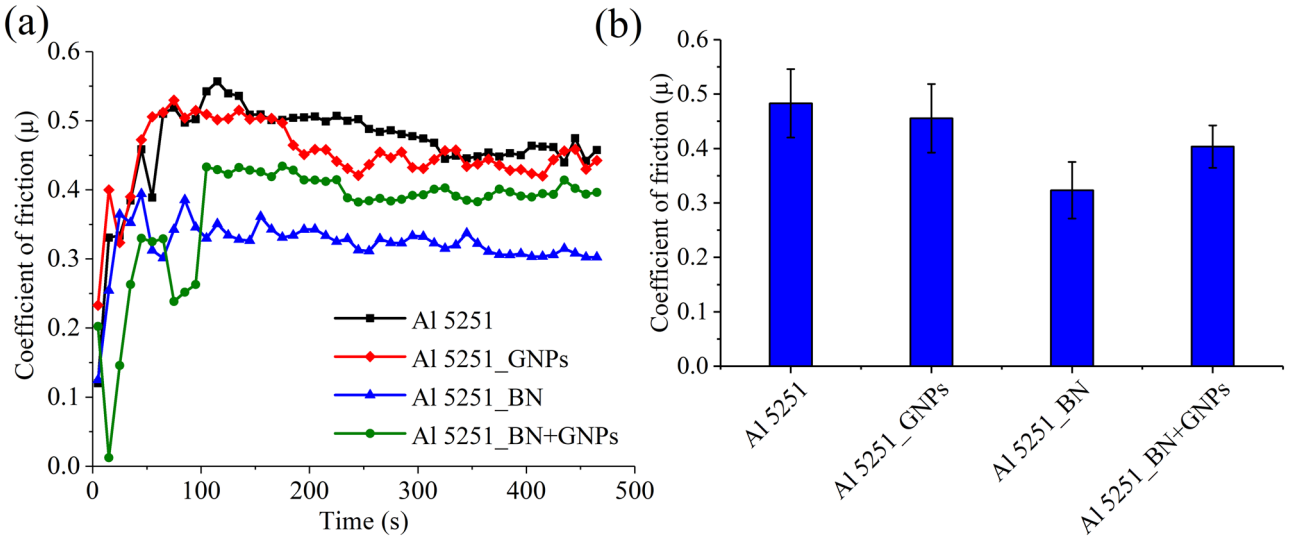


**Figure 10:** Behaviour of the COF with the time of the fabricated composites.

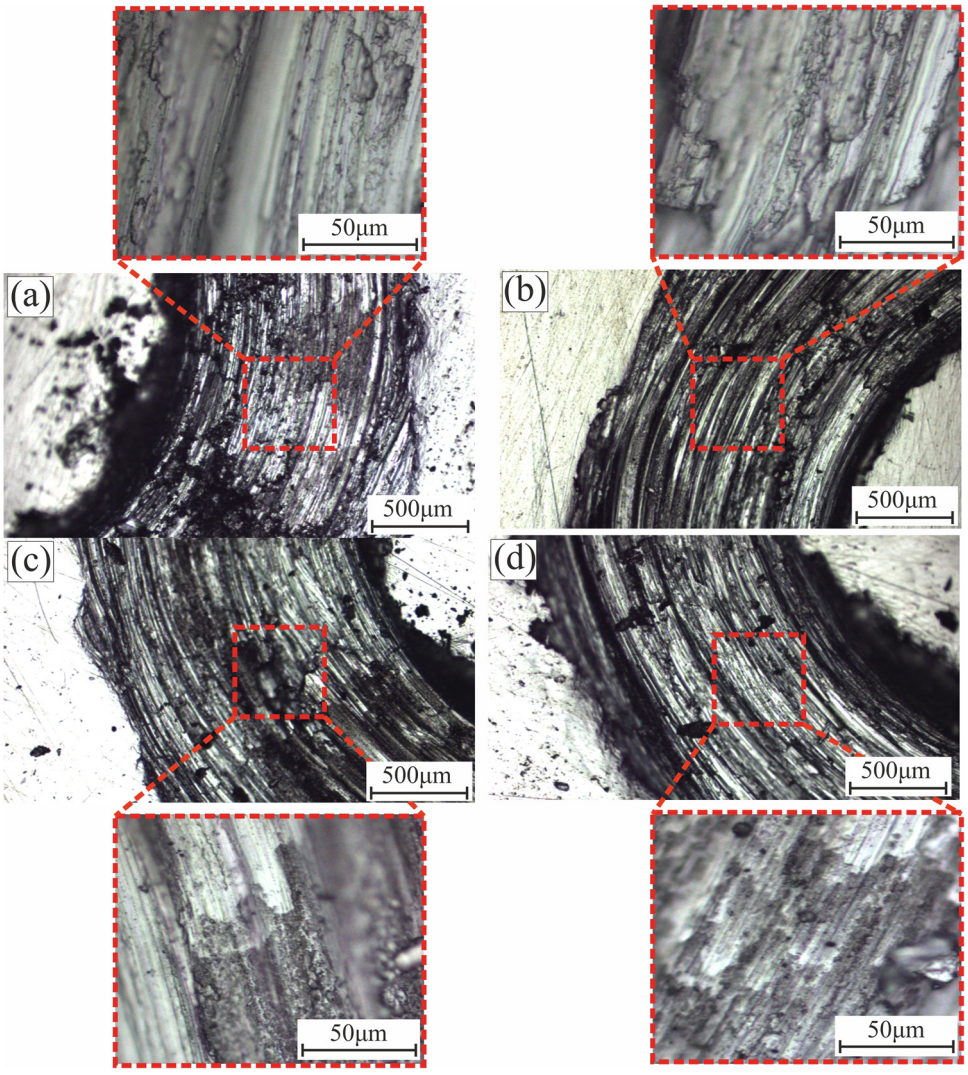


**Figure 11:** Microscopy image of the worn tracks of the tested samples using a tribometer tester: (a) as-received Al 5251 alloy, (b) Al 5251_GNPs composite, (c) Al 5251_BN composite, and (d) Al 5251_BN + GNPs composite.

reinforcement particles are incorporated into the nanocomposite matrix and they increase the wear resistance.

The surfaces for the ploughing tracks generated during the dry wear sliding path are presented in Figure 11. The following are the fabricated composites: Al 5251_GNPs, Al 5251_BN, and Al 5251_BN + GNPs composites. According to the worn surfaces with high-magnification images for the investigated samples, the Al 5251 alloy wear surface demonstrated delamination and massive exfoliation, causing extreme wear (Figure 11a). The worn surfaces for Al 5251_BN (Figure 11c) and Al 5251_BN + GNPs (Figure 11d) were cleaner than that for Al 5251_GNPs (Figure 11b), and the base alloy Al 5251 resulted in the nanocomposite having a lower wear rate.

Figure 12 compares the cross-sections of the wear track width profiles between the as-received Al 5251 alloy and the fabricated surface nanocomposites. The Al 5251 alloy exhibited a better larger wear profile than all composites. With the addition of mono BN nanoparticles, mono GNPs, and a hybrid of BN nanoparticles and GNPs, the wear penetration depth was decreased to approximately 45, 25, and 35 μm at 10 N load, respectively (Figure 12). There was material uplift on the inside and outside circumferences of the wear track profiles because of the steel pin penetrating the material, causing plastic deformation.

The experimental wear rate by volume loss and weight loss rates of the base Al 5251 and fabricated composites is presented in Figure 13. Using the volume loss method (Figure 13a) and weight loss method (Figure 13b), the wear rate was expectedly improved by reinforcing the studied alloy by BN nanoparticles and GNPs into the base matrix. The Al 5251 alloy exhibits a wear volume loss of

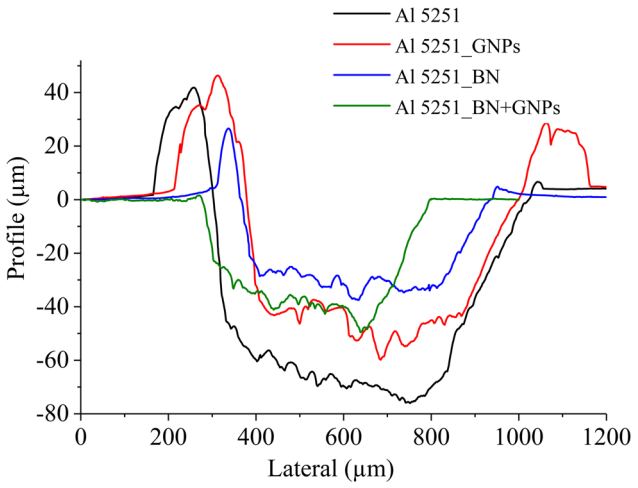


**Figure 12:** Wear profile of the investigated samples under a constant load of 10 N.

0.069 $mm^3$ and a wear rate by weight loss of 0.0175 mg/s at a 10 N load. As explained above, BN nanoparticles play a significant role in enhancing the wear performance of the nanocomposite matrix. The mono GNPs insignificantly improve the tribological behaviour of Al 5251 alloy, while reinforcing a hybrid of GNPs and BN nanoparticles is a feasible approach for improving the action of GNPs. The results of the two wear methods differ in terms of the behaviour and mechanism of each test. Hence, the volume wear method depends on the extent to which the wear tool scratches the sample during the test. It is determined by the operation of a circular path and depends on the material strength; thus, if the composite matrix is not fully homogeneous and the reinforced particles are not distributed well, the wear results will be affected. In contrast, in the weight loss method, full friction contact to the sample surface is maintained. Hence, in the case of the weight loss method, the reinforced particles and metal matrix are subjected to wear action.

## 4 Conclusion

1) FSP transformed the elongated coarse-grained structure of the base Al 5251 alloy into an equiaxed and four times finer structure, with the mean grain size being decreased from 60 to 15 μm. The reinforcement nanoparticles (GNPs and BN nanoparticles) increased the refining effect. Hence, the mean grain size decreased to 11 μm for GNP reinforcement, 12 μm for BN reinforcement, and 13 μm for hybrid GNP/BN reinforcement.
2) The BN nanocomposites provided a superior wear resistance compared to the base alloy and other composites. The GNPs insignificantly enhanced the wear resistance due to their lubricating nature and the composite morphology difference. The wear resistance of the hybrid nanocomposite was enhanced by 40% compared to that of the base alloy. The integration between GNPs and BN particles in the Al matrix helped improve the mechanical and wear behavior of fabricated nanocomposites.

a. FSP increased the hardness of the as-received Al 5251 alloy by 20%. Reinforcing the surface by the BN nanoparticles, GPNs and a hybrid of nanoparticles + GNPs increased the hardness by 120, 50, and 80%, respectively.

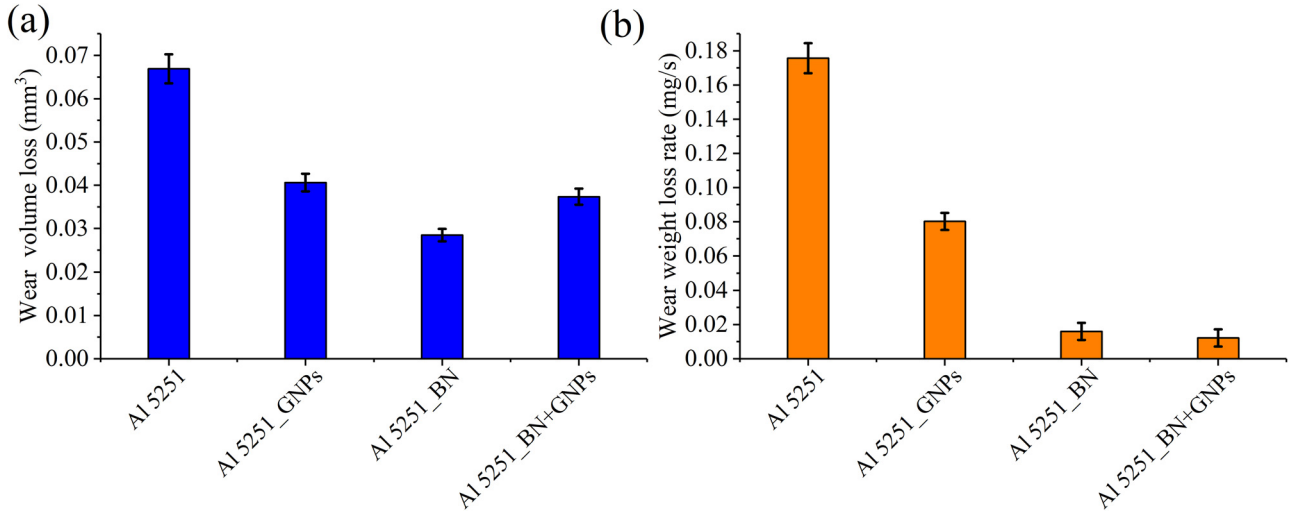


**Figure 13:** (a) Wear volume loss and (b) the wear weight-loss rate.

3) The Al 5251_BN nanocomposite showed superior wear resistance among the investigated composites due to good uniform dispersion and homogeneity in the composite matrix during FSP. Although both BN particles and GNPs exhibit the same lubricating properties, GNPs' morphology causes some irregular distribution of these particles during the stirring action. In contrast, the BN nanoparticles were distributed well in such a way to make the matrix resist the applied wear. The dependency criterion between hardness and resistance to wear was not found to be much reliable when investigating and comparing the mono and hybrid composites.
4) The mechanical properties obtained after FSP were improved in terms of both grain boundary (finer grains and more grain boundaries) and nanoparticle dispersion strengthening mechanisms. Al 5251/GNP nanocomposites exhibited the most significant yield and ultimate tensile strengths, which were 110 and 60% greater than those of the base metal. In contrast, the plasticity was decreased to 40% elongation to failure. The more improvement in the mechanical properties of Al 5251/GNPs and Al 5251/GNPs_BN is attributed to the large specific surface area of GNPs, which led to good interfacial adhesion between the AMMC and the reinforcements.

**Acknowledgment:** The authors extend their appreciation to the Deputyship of Research & Innovation, Ministry of Education in Saudi Arabia for funding this research work through the project number (IFPRC-201-135-2020) and King Abdulaziz University, Jeddah, Saudi Arabia.

**Funding information:** This research work was funded by an institutional fund project under grant no IFPRC-201-135-2020. The authors gratefully acknowledge technical and financial support from the ministry of education and King Abdulaziz University, DSR, Jeddah, Saudi Arabia.

**Author contributions:** All authors have accepted responsibility for the entire content of this manuscript and approved its submission.

**Conflict of interest:** The authors state no conflict of interest.

# References

[1] Kumar HGP, Xavior MA. Graphene reinforced metal matrix composite (GRMMC): a review. Proc Eng. 2014;97:1033–40.
[2] AbuShanab WS, Moustafa EB, Ghandourah E, Taha MA. Effect of graphene nanoparticles on the physical and mechanical properties of the Al2024-graphene nanocomposites fabricated by powder metallurgy. Results Phys. 2020;19:103343.
[3] Sharma A, Sharma VM, Paul J. Fabrication of bulk aluminum-graphene nanocomposite through friction stir alloying. J Composite Mater. 2019;54(1):45–60.
[4] Xiang S, Wang X, Gupta M, Wu K, Hu X, Zheng M. Graphene nanoplatelets induced heterogeneous bimodal structural magnesium matrix composites with enhanced mechanical properties. Sci Rep. 2016;6:38824.
[5] Moustafa EB, Taha MA. Preparation of high strength graphene reinforced Cu-based nanocomposites via mechanical alloying method: microstructural, mechanical and electrical properties. Appl Phys A. 2020;126(3):220.
[6] Li M, Zhang Z, Gao H, Wang Y, Liang J, Shu D, et al. Formation of multilayer interfaces and the load transfer in graphene nanoplatelets reinforced Al matrix composites. Mater Charact. 2020;159:110018.
[7] Tabandeh-Khorshid M, Ajay K, Omrani E, Kim C, Rohatgi P. Synthesis, characterization, and properties of graphene reinforced metal-matrix nanocomposites. Compos Part B Eng. 2020;13:107664.
[8] Khorshid MT, Jahromi SAJ, Moshksar MM. Mechanical properties of tri-modal Al matrix composites reinforced by nano- and submicron-sized $Al_2O_3$ particulates developed by wet attrition milling and hot extrusion. Mater Des. 2010;31(8):3880–4.
[9] Jeon C-H, Jeong Y-H, Seo J-J, Tien HN, Hong S-T, Yum Y-J, et al. Material properties of graphene/aluminum metal matrix composites fabricated by friction stir processing. Int J Precis Eng Manuf. 2014;15(6):1235–9.
[10] Bhimanapati GR, Lin Z, Meunier V, Jung Y, Cha J, Das S, et al. Recent advances in two-dimensional materials beyond graphene. ACS Nano. 2015;9(12):11509–39.
[11] Xue Y, Jiang B, Bourgeois L, Dai P, Mitome M, Zhang C, et al. Aluminum matrix composites reinforced with multi-walled boron nitride nanotubes fabricated by a high-pressure torsion technique. Mater Des. 2015;88:451–60.
[12] Gostariani R, Ebrahimi R, Asadabad MA, Paydar MH. Mechanical properties of Al/BN nanocomposites fabricated by planetary ball milling and conventional hot extrusion. Acta Metall Sin (Engl Lett). 2017;31(3):245–53.
[13] Bhat A, Budholiya S, Aravind Raj S, Sultan MTH, Hui D, Md Shah AU, et al. Review on nanocomposites based on aerospace applications. Nanotechnol Rev. 2021;10(1):237–53.
[14] Paidar M, Asgari A, Ojo OO, Saberi A. Mechanical properties and wear behavior of AA5182/WC nanocomposite fabricated by friction stir welding at different tool traverse speeds. J Mater Eng Perform. 2018;27(4):1714–24.
[15] Mondal S. Aluminum or its alloy matrix hybrid nanocomposites. Met Mater Int. 2021;27:2188–204.
[16] Arab M, Marashi SPH. Graphene nanoplatelet (GNP)-incorporated AZ31 magnesium nanocomposite: microstructural, mechanical and tribological properties. Tribol Lett. 2018;66:4.
[17] Harish TM, Mathai S, Cherian J, Mathew KM, Thomas T, Vishnu Prasad KV, et al. Development of aluminium 5056/SiC/bagasse ash hybrid composites using stir casting method. Mater Today Proc. 2020;27:2635–9.
[18] Moustafa E, Mohammed S, Abdel-Wanis S, Mahmoud T, El-Kady ES. Review multi pass friction stir processing. Am Sci Res J Eng Technol Sci. 2016;22(1):98–108.

[19] Eskandari H, Taheri R. A novel technique for development of aluminum alloy matrix/$TiB_2$/$Al_2O_3$ hybrid surface nanocomposite by friction stir processing. Proc Mater Sci. 2015;11:503–8.
[20] Gan YX, Solomon D, Reinbolt M. Friction stir processing of particle reinforced composite materials. Materials. 2010;3(1):329–50.
[21] Moustafa E. Effect of multi-pass friction stir processing on mechanical properties for AA2024/$Al_2O_3$ nanocomposites. Mater (Basel). 2017;10:9.
[22] Moustafa EB, Mosleh AO. Effect of (Ti–B) modifier elements and FSP on 5052 aluminum alloy. J Alloy Compd. 2020;153745.
[23] Tang J, Shen Y, Li J. Influences of friction stir processing parameters on microstructure and mechanical properties of SiC/Al composites fabricated by multi-pin tool. J Manuf Process. 2019;38:279–89.
[24] Kurt HI. Influence of hybrid ratio and friction stir processing parameters on ultimate tensile strength of 5083 aluminum matrix hybrid composites. Compos Part B Eng. 2016;93:26–34.
[25] Sahraeinejad S, Izadi H, Haghshenas M, Gerlich AP. Fabrication of metal matrix composites by friction stir processing with different particles and processing parameters. Mater Sci Eng A. 2015;626:505–13.
[26] Me B. Dynamic characteristics study for surface composite of AMMNCs matrix fabricated by friction stir process. Materials (Basel). 2018;11:7
[27] Essam B, Moustafa SM, Tamer M, Sayed A, El-Sayed E. Surface composite defects of Al/$Al_2O_3$ metal matrix fabricated by friction stir processing. J Mater Sci Surf Eng. 2017;5(2):524–7.
[28] Moustafa E. Effect of multi-pass friction stir processing on mechanical properties for AA2024/Al(2)O(3) nanocomposites. Materials. 2017;10(9):1053.
[29] Pol N, Verma G, Pandey RP, Shanmugasundaram T. Fabrication of AA7005/TiB2-B4C surface composite by friction stir processing: evaluation of ballistic behaviour. Def Technol. 2019;15(3):363–8.
[30] Rasagopal P, Senthilkumar P, Magibalan S, Nallakumarasamy G. A study surface integrity of aluminum hybrid composites during milling operation. J Mater Res Technol. 2020;9(3):4884–93.
[31] Kalaf O, Nasir T, Asmael M, Safaei B, Zeeshan Q, Motallebzadeh A, et al. Friction stir spot welding of AA5052 with additional carbon fiber-reinforced polymer composite interlayer. Nanotechnol Rev. 2021;10(1):201–9.
[32] Hosseini SA, Ranjbar K, Dehmolaei R, Amirani AR. Fabrication of Al5083 surface composites reinforced by CNTs and cerium oxide nano particles via friction stir processing. J Alloy Compd. 2015;622:725–33.
[33] Moustafa EB. Hybridization effect of BN and $Al_2O_3$ nanoparticles on the physical, wear, and electrical properties of aluminum AA1060 nanocomposites. Appl Phys A. 2021;127:9.
[34] ASTM. Standard test methods for tension testing wrought and cast aluminum- and magnesium-alloy products. West Conshohocken, PA: ASTM International; 2015.
[35] Mouritz AP. Aluminium alloys for aircraft structures. Introduction to aerospace materials. Cambridge, UK: Woodhead Publishing; 2012. p. 173–201.
[36] Mucelin KJ, Gonçalves PdC, Hammes G, Binder R, Janssen R, Klein AN, et al. Tribological study of self-lubricating composites with hexagonal boron nitride and graphite as solid lubricants. ABM Proceedings; 2014. p. 3772–81.
[37] Menezes PL, Kishore, Kailas SV. Studies on friction and transfer layer using inclined scratch. Tribol Int. 2006;39(2):175–83.
[38] Cowap MJH, Moghaddam SRM, Menezes PL, Beschorner KE. Contributions of adhesion and hysteresis to coefficient of friction between shoe and floor surfaces: effects of floor roughness and sliding speed. Tribol Mater Surf Interfaces. 2015;9(2):77–84.
[39] Shen Q, Shi X, Zou J, Yang K, Huang Y, Zhang A, et al. Tribological performance and self-lubricating film formation mechanism of TiAl-based composites at elevated temperatures. J Mater Eng Perform. 2016;26(1):268–76.